A Shape Optimization Method for Nonlinear Axisymmetric Magnetostatics Using a Coupling of Finite and Boundary Elements *

Dalibor Lukáš†, Kamil Postava and Ondřej Životský‡

Abstract

In this paper we propose a method for constrained shape optimization governed with a nonlinear axisymmetric magnetostatic state problem and we apply it to an optimal shape design of an electromagnet. The state problem is solved via Hiptmair's symmetric coupling of finite elements employed in the interior ferromagnetic domain and boundary elements modelling the exterior air domain as well as current excitations. The boundary element integrals are regularized by a Duffy transform and evaluated then using a tensor–product Gaussian quadrature. Nonlinear ferromagnetic behaviour is resolved by Newton iterations. The optimization method under both linear and nonlinear constraints relies on the steepest–descent search, projections onto the set of linearized constraints, and an adjoint method of shape sensitivity analysis. Shape perturbations influence grid deformation via a solution to an auxiliary torsion–free linear elasticity problem. Finally, numerical results are presented.

Keywords: shape optimization, nonlinear magnetostatics, boundary element method, finite element method, adjoint sensitivity analysis

1 Introduction

Shape optimization has become a standard computing tool in both research and engineering design. It concerns on minimization of a given quantity, called cost functional, under some restrictions, called constraints, so that their evaluation involves a computation of a physical field typically described by partial differential equations, called state problem, over geometrical domains the

*This work was supported by the Czech Ministry of Education under the project MSM6198910027 and by the Czech Academy of Science under the project AVČR 1ET400300415. Partial support from the projects KAN 400100653 and from the Grant Agency of the Czech Republic (202/06/0531) is acknowledged.

†Department of Applied Mathematics, VŠB–Technical University of Ostrava, Czech Republic, email: dalibor.lukas@vsb.cz

‡Department of Physics, VŠB–Technical University of Ostrava, Czech Republic, emails: kamil.postava@vsb.cz, ondrej.zivotsky@post.cz

shape or interfaces of which are variable. There is a couple of classification of shape optimization methods. One class of methods [HN97] approximates the original inifinite–dimensional optimization problem by a sequence of its finite–dimensional counterparts. Then, necessary optimality (Karush–Kuhn–Tucker) conditions for the subproblems are formulated separately in terms of linear algebra and gradient–type solution methods are employed. Another approach [SZ92] aims to develop first an infinite–dimensional setting of the necessary optimality conditions in terms of shape derivatives and then discretize them properly. For some problems one can even derive sufficient optimality conditions in terms of a shape Hessian in the infinite–dimension and prove its coercivity [Epp00], in order to employ Newton–type optimization methods. A nice property of the latter methods is that the optimality conditions are formulated along the design boundary or interface. This leads to a superior use of boundary element methods (BEM) [EH06], which discretizes only the boundary, rather than volume discretizations in case of finite element methods (FEM).

In contrary to FEM discretizations, BEM arise in densely populated linear systems. Moreover, BEM systems are assembled from singular integrals, which hardly have closed forms. Until recently, these drawbacks have made BEM less frequently used comparing to FEM. Fortunately, there have been developed regularization techniques [Duf82, SS97, SS04] that transform singular integrands into analytic functions and integrate them efficiently by a low–order Gaussian quadrature afterwards. There also has been made a great progress in development on sparsification of the dense systems [Rok85, HN89, Beb00, RS07], which enables them to solve in an almost optimal computational complexity.

The nonlinear state problem under our consideration cannot be solved by a pure BEM, but rather a FEM–BEM coupling. A symmetric FEM–BEM scheme was first proposed in [Cos87]. In case of magnetostatics, one can employ the scalar magnetic potential in the air domain and the vector ansatz in ferromagnetics and coil domains, cf. [KS02], but then an FEM discretization of coils is necessary. Here, we prefer to use the ansatz of [Hip02], which is based on the Stratton–Chu representation formula for the eddy current case of Maxwell's equations and where coils excitation is included in BEM.

The aim of this paper is to bring the recent BEM formulation of eddy currents problem [Hip02], the ideas behind Gauss quadrature of BEM kernels [SS04], and our latest development of adjoint techniques for shape sensitivity analysis [LC07] together and apply it to a problem of optimal shape design in nonlinear magnetostatics. In particular, the presented application of an electromagnet is useful for nondestructive observation of magnetic domains [HS98, Pos02] and development of new magnetic and optical recording media. The paper is organized as follows: In Section 2 we recall a symmetric FEM–BEM coupling for nonlinear magnetostatics, reduce it due to the axial symmetry and derive regularizations of Cauchy–singular integrands to justify Gaussian quadrature. In Section 3 we introduce an abstract setting of a shape optimization problem, describe evaluation of cost and constraint functions for the finite–dimensional counterparts. Further we propose a steepest–descent optimization method with an active–set treatment of both linear and nonlinear

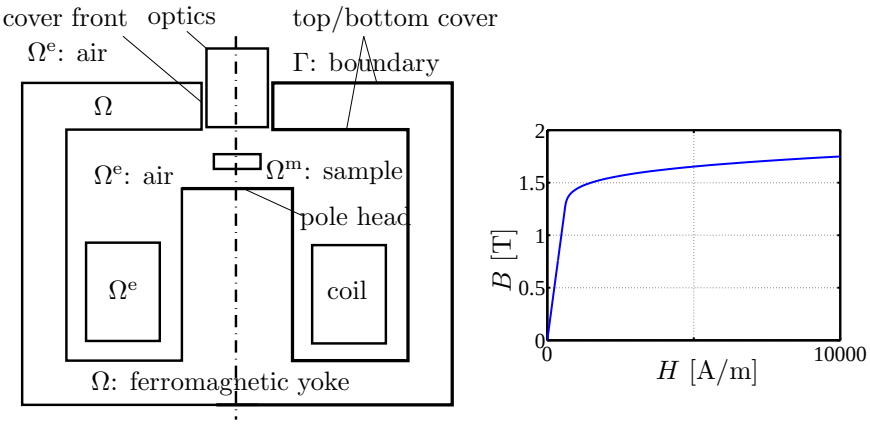

Figure 1: Axisymmetric geometry of the electromagnet (left), B–H curve of the used soft magnetic iron AREMA (right)

constraints and describe an adjoint algebraic method of shape sensitivity analysis. In Section 4 we give numerical results for an optimization of an electromagnet and discuss convergence properties of the algorithm.

2 State problem

We consider the geometry of a direct electric current electromagnet that is depicted in Fig. 1 (left). Let $\Omega \subset \mathbb{R}^3$ be a simply connected Lipschitz domain occupied by ferromagnetic parts, where the unit outward normal to $\Gamma := \partial\Omega$ is denoted by $\mathbf{n}$. Denote by $\Omega^{\mathrm{e}} := \mathbb{R}^3 \setminus \overline{\Omega}$ the domain occupied by air and coils. Further, let $\mathbf{u}$ and $\mathbf{u}^{\mathrm{e}}$ stand for the magnetic vector potentials defined in Ω and Ω^{e}, respectively, $\nu_0 := 1/(4\pi 10^{-7})$ and $\nu_{\mathrm{r}}(t)$ be the constant air reluctivity and the nonlinear ferromagnetic reluctivity function determining the so–called B–H curve by $H = \nu_r(B)\, B$, see Fig. 1 (right), respectively, and let $\mathbf{J}$ denote a divergence–free current density function compactly supported in Ω^{e}. Then the magnetostatic state problem under consideration reads as follows:

$$
\begin{aligned}
\mathbf{curl}\,(\nu_{\mathrm{r}}(\|\mathbf{curl}\,\mathbf{u}\|)\,\mathbf{curl}\,\mathbf{u}) &= \mathbf{0} && \text{in } \Omega,\\
\operatorname{div}\mathbf{u} &= 0 && \text{in } \Omega,\\
\mathbf{curl}\,\mathbf{curl}\,\mathbf{u}^{\mathrm{e}} &= \mathbf{J}/\nu_0 && \text{in } \Omega^{\mathrm{e}},\\
\operatorname{div}\mathbf{u}^{\mathrm{e}} &= 0 && \text{in } \Omega^{\mathrm{e}},\\
\mathbf{n}\times((\mathbf{u}-\mathbf{u}^{\mathrm{e}})\times\mathbf{n}) &= \mathbf{0} && \text{on } \Gamma,\\
\left(\nu_{\mathrm{r}}(\|\mathbf{curl}\,\mathbf{u}\|^2)\,\mathbf{curl}\,\mathbf{u} - \mathbf{curl}\,\mathbf{u}^{\mathrm{e}}\right)\times\mathbf{n} &= \mathbf{0} && \text{on } \Gamma,\\
\mathbf{u}^{\mathrm{e}}(\mathbf{x}) &= O(\|\mathbf{x}\|^{-1}) && \text{at } \infty.
\end{aligned}
\tag{1}
$$

We will approximate the solution to (1) by a coupling of FEM and BEM in order to avoid typical troubles arising in pure FEM discretizations, such as: a hardly estimated error of an artificial domain truncation, a related large number

of degrees of freedom in the truncated exterior domain, and deteoriating shapes of exterior elements due to grid deformations within shape optimization. The following coupled FEM–BEM discretizes only the interior domain Ω.

2.1 Symmetric FEM–BEM method

To formulate the system (1) in a variational framework, we apply the ansatz introduced and rigorously analyzed by Hiptmair in [Hip02]. It is based on the following Stratton–Chu representation formula for the exterior field:

$$\mathbf{u}^{\mathrm{e}} = \boldsymbol{\Psi}_{\mathrm{M}}\left(\boldsymbol{\gamma}_{\mathrm{D}}^{\mathrm{e}}\mathbf{u}^{\mathrm{e}}\right) - \boldsymbol{\Psi}_{\mathrm{A}}\left(\boldsymbol{\gamma}_{\mathrm{N}}^{\mathrm{e}}\mathbf{u}^{\mathrm{e}}\right) - \nabla\Psi_{\mathrm{V}}\left(\boldsymbol{\gamma}_{\mathbf{n}}^{\mathrm{e}}\mathbf{u}^{\mathrm{e}}\right) + \mathbf{G}(\mathbf{J}/\nu_0), \tag{2}$$

where we respectively consider the following Dirichlet, Neumann, and normal exterior trace operators on Γ: $\boldsymbol{\gamma}_{\mathrm{D}}^{\mathrm{e}}\mathbf{u}^{\mathrm{e}}(\mathbf{y}) := \mathbf{n}(\mathbf{y}) \times (\mathbf{u}^{\mathrm{e}}(\mathbf{y}) \times \mathbf{n}(\mathbf{y}))$, $\boldsymbol{\gamma}_{\mathrm{N}}^{\mathrm{e}}\mathbf{u}^{\mathrm{e}}(\mathbf{y}) := \mathbf{curl}(\mathbf{u}^{\mathrm{e}}(\mathbf{y})) \times \mathbf{n}(\mathbf{y})$, and $\boldsymbol{\gamma}_{\mathbf{n}}^{\mathrm{e}}\mathbf{u}^{\mathrm{e}}(\mathbf{y}) := \mathbf{u}^{\mathrm{e}}(\mathbf{y}) \cdot \mathbf{n}(\mathbf{y})$, and where, for $\mathbf{x} \notin \Gamma$, we define the scalar single layer potential by

$$\Psi_{\mathrm{V}}\left(\phi(\mathbf{y})\right)(\mathbf{x}) := \int_{\Gamma} \phi(\mathbf{y}) E(\mathbf{x},\mathbf{y})\, dS(\mathbf{y}),$$

the vectorial single layer potential by

$$\boldsymbol{\Psi}_{\mathrm{A}}\left(\boldsymbol{\lambda}(\mathbf{y})\right)(\mathbf{x}) := \int_{\Gamma} \boldsymbol{\lambda}(\mathbf{y}) E(\mathbf{x},\mathbf{y})\, dS(\mathbf{y}),$$

the vectorial double layer potential by

$$\boldsymbol{\Psi}_{\mathrm{M}}\left(\mathbf{u}(\mathbf{y})\right)(\mathbf{x}) := \mathbf{curl}\left(\boldsymbol{\Psi}_{\mathrm{A}}\left(\mathbf{n}(\mathbf{y}) \times \mathbf{u}(\mathbf{y})\right)\right),$$

and the vectorial Newton potential by

$$\mathbf{G}\left(\boldsymbol{\lambda}(\mathbf{y})\right)(\mathbf{x}) := \int_{\mathbb{R}^3} \boldsymbol{\lambda}(\mathbf{y}) E(\mathbf{x},\mathbf{y})\, dS(\mathbf{y}),$$

where, for $\mathbf{x} \neq \mathbf{y}$, $E(\mathbf{x},\mathbf{y}) := 1/\left(4\pi\|\mathbf{x}-\mathbf{y}\|\right)$ denotes the Laplace kernel.

Now we can formally apply both the Dirichlet and Neumann exterior trace operators to (2) and we arrive at a system of two equations, however, for three unknown boundary data: $\boldsymbol{\gamma}_{\mathrm{D}}^{\mathrm{e}}\mathbf{u}^{\mathrm{e}}$, $\boldsymbol{\gamma}_{\mathrm{N}}^{\mathrm{e}}\mathbf{u}^{\mathrm{e}}$, and $\boldsymbol{\gamma}_{\mathbf{n}}^{\mathrm{e}}\mathbf{u}^{\mathrm{e}}$. In case of magnetostatics, we are not interested in the latter. To get rid of it, namely of the only term $\boldsymbol{\gamma}_{\mathrm{D}}^{\mathrm{e}}\left(\nabla\Psi_{\mathrm{V}}\left(\boldsymbol{\gamma}_{\mathbf{n}}^{\mathrm{e}}\mathbf{u}^{\mathrm{e}}\right)\right)$, in [Hip02] it is proposed to test the second equation against functions in the Sobolev space

$$\boldsymbol{\Lambda} := \mathbf{H}_{||}^{-1/2}\left(\mathrm{div}_{\Gamma} 0; \Gamma\right) := \left\{\boldsymbol{\lambda} \in \mathbf{H}_{||}^{-1/2}(\Gamma) \ : \ \mathrm{div}_{\Gamma}\boldsymbol{\lambda} = \mathbf{0}\right\}, \tag{3}$$

where div_{Γ} denotes the surface divergence operator and where $\mathbf{H}_{||}^{-1/2}(\Gamma)$ is the dual space to a space of tangential surface vector fields defined and analyzed in [BC01a]. Additionaly, from [BC01a] we need yet another Sobolev space

$$\mathbf{W} := \mathbf{H}_{\perp}^{-1/2}\left(\mathrm{curl}_{\Gamma}; \Gamma\right) := \left\{\mathbf{v} \in \mathbf{H}_{\perp}^{-1/2}(\Gamma) \ : \ \mathrm{curl}_{\Gamma}\mathbf{v} \in H^{-1/2}(\Gamma)\right\}, \tag{4}$$

where curl_Γ denotes the surface scalar rotation operator and where $\mathbf{H}_\perp^{-1/2}(\Gamma)$ is the dual space to a space of normal surface vector fields. It is proved in [BC01b] that $\mathbf{H}_{||}^{-1/2}(\Gamma)$ and $\mathbf{H}_\perp^{-1/2}(\Gamma)$ are dual to each other and we denote the duality pairing by $\langle .,. \rangle_\Gamma$. Let us introduce $\mathbf{A}(\boldsymbol{\lambda}) := \boldsymbol{\gamma}_{\mathrm{D}}^{\mathrm{e}} \boldsymbol{\Psi}_{\mathrm{A}}(\boldsymbol{\lambda})$, $\mathbf{B}(\boldsymbol{\lambda}) := \boldsymbol{\gamma}_{\mathrm{N}}^{\mathrm{e}} \boldsymbol{\Psi}_{\mathrm{A}}(\boldsymbol{\lambda})$, $\mathbf{C}(\mathbf{v}) := \boldsymbol{\gamma}_{\mathrm{D}}^{\mathrm{e}} \boldsymbol{\Psi}_{\mathrm{M}}(\mathbf{v})$, and $\mathbf{N}(\mathbf{v}) := \boldsymbol{\gamma}_{\mathrm{N}}^{\mathrm{e}} \boldsymbol{\Psi}_{\mathrm{M}}(\mathbf{v})$. Now, by applying the Dirichlet and Neumann trace operators to (2) and testing the equations against (3) and (4), respectively, we arrive at the following so–called exterior Calderón projector in weak form [Hip02]:

$$\begin{aligned} \langle \boldsymbol{\xi}, \boldsymbol{\gamma}_{\mathrm{D}}^{\mathrm{e}} \mathbf{u}^{\mathrm{e}} \rangle_\Gamma &= \langle \boldsymbol{\xi}, \mathbf{C}\left(\boldsymbol{\gamma}_{\mathrm{D}}^{\mathrm{e}} \mathbf{u}^{\mathrm{e}}\right) \rangle_\Gamma - \langle \boldsymbol{\xi}, \mathbf{A}\left(\boldsymbol{\gamma}_{\mathrm{N}}^{\mathrm{e}} \mathbf{u}^{\mathrm{e}}\right) \rangle_\Gamma + \langle \boldsymbol{\xi}, \boldsymbol{\gamma}_{\mathrm{D}}^{\mathrm{e}} \mathbf{G}(\mathbf{J}/\nu_0) \rangle_\Gamma, \\ \langle \boldsymbol{\gamma}_{\mathrm{N}}^{\mathrm{e}} \mathbf{u}^{\mathrm{e}}, \mathbf{w} \rangle_\Gamma &= \langle \mathbf{N}\left(\boldsymbol{\gamma}_{\mathrm{D}}^{\mathrm{e}} \mathbf{u}^{\mathrm{e}}\right), \mathbf{w} \rangle_\Gamma - \langle \mathbf{B}\left(\boldsymbol{\gamma}_{\mathrm{N}}^{\mathrm{e}} \mathbf{u}^{\mathrm{e}}\right), \mathbf{w} \rangle_\Gamma + \langle \boldsymbol{\gamma}_{\mathrm{N}}^{\mathrm{e}} \mathbf{G}(\mathbf{J}/\nu_0), \mathbf{w} \rangle_\Gamma, \end{aligned}$$

solved for $(\boldsymbol{\gamma}_{\mathrm{D}}^{\mathrm{e}} \mathbf{u}^{\mathrm{e}}, \boldsymbol{\gamma}_{\mathrm{N}}^{\mathrm{e}} \mathbf{u}^{\mathrm{e}}) \in \mathbf{W} \times \boldsymbol{\Lambda}$ and tested for all $(\mathbf{w}, \boldsymbol{\xi}) \in \mathbf{W} \times \boldsymbol{\Lambda}$. Finally, applying Green's formula to the first equation in (1) and using the Neumann transmission condition on Γ, see (1), we arrive at the coupled variational problem: Find $\mathbf{u} \in \mathbf{V} := \mathbf{H}(\mathbf{curl}; \Omega)$ and $\boldsymbol{\lambda} := \boldsymbol{\gamma}_{\mathrm{N}}^{\mathrm{e}} \mathbf{u}^{\mathrm{e}} \in \boldsymbol{\Lambda}$:

$$\begin{array}{rcrcl} q(\mathbf{u}; \mathbf{u}, \mathbf{v}) - \langle \mathbf{N}(\boldsymbol{\gamma}_{\mathrm{D}} \mathbf{u}), \boldsymbol{\gamma}_{\mathrm{D}} \mathbf{v} \rangle_\Gamma & + & \langle \mathbf{B}(\boldsymbol{\lambda}), \boldsymbol{\gamma}_{\mathrm{D}} \mathbf{v} \rangle_\Gamma & = & \langle \boldsymbol{\gamma}_{\mathrm{N}}^{\mathrm{e}} \mathbf{G}(\mathbf{J}/\nu_0), \boldsymbol{\gamma}_{\mathrm{D}} \mathbf{v} \rangle_\Gamma, \\ -\langle \mathbf{B}(\boldsymbol{\xi}), \boldsymbol{\gamma}_{\mathrm{D}} \mathbf{u} \rangle_\Gamma & + & \langle \boldsymbol{\xi}, \mathbf{A}(\boldsymbol{\lambda}) \rangle_\Gamma & = & \langle \boldsymbol{\xi}, \boldsymbol{\gamma}_{\mathrm{D}}^{\mathrm{e}} \mathbf{G}(\mathbf{J}/\nu_0) \rangle_\Gamma, \end{array} \tag{5}$$

tested for $(\mathbf{v}, \boldsymbol{\xi}) \in \mathbf{V} \times \boldsymbol{\Lambda}$, where $q(\mathbf{w}; \mathbf{u}, \mathbf{v}) := \int_\Omega \nu_r(\|\mathbf{curl}\, \mathbf{w}\|) \mathbf{curl}\, \mathbf{u} \cdot \mathbf{curl}\, \mathbf{v}\, d\mathbf{x}$ and $\boldsymbol{\gamma}_{\mathrm{D}}$ denotes the interior Dirichlet trace operator. In [Hip02] the well–posedness of (5) is proved in case of a constant ν_{r}. In the nonlinear case we additionaly have to assume the strong monotonicity of ν_{r}, i.e.,

$$\exists c_\nu > 0 \; \forall s, t \geq 0 : \; (\nu_{\mathrm{r}}(s) s - \nu_{\mathrm{r}}(t) t)\,(s - t) \geq c_\nu (s - t)^2, \tag{6}$$

as well as its Lipschitz continuity, i.e.,

$$\exists C_\nu > 0 \; \forall s, t \geq 0 : \; |\nu_{\mathrm{r}}(s) s - \nu_{\mathrm{r}}(t) t| \leq C_\nu |s - t|. \tag{7}$$

In case of magnetostatics both (6) and (7) are naturally fulfilled [Pec04]. The well–posedness follows from the nonlinear Lax–Milgram theorem, cf. [Nec83].

A FEM–BEM method is now given via the Galerkin approximation of (5) on $\mathbf{V}_h \times \boldsymbol{\Lambda}_h \subset \mathbf{V} \times \boldsymbol{\Lambda}$ so that $\mathbf{V}$ is discretized using first–order edge elements [Ned80] in Ω and $\boldsymbol{\Lambda}$ using the divergence–free lowest order Raviart–Thomas elements on Γ, namely, $\boldsymbol{\Lambda}_h := \mathbf{curl}_\Gamma \mathcal{S}_1(\Gamma)$, where $\mathcal{S}_1(\Gamma)$ is the first–order nodal FEM–space on Γ and $\mathbf{curl}_\Gamma v := \mathbf{n} \times \nabla \widetilde{v}$, provided a proper extension $\widetilde{v}$ of v from Γ.

2.2 Axisymmetric case

Referring to Fig. 1 (left), assume an axisymmetric geometry, i.e. $\omega := \{(r, z) \in \mathbb{R}^2 \; : \; \mathbf{x}(r, z, t) \in \Omega\}$, where $\mathbf{x}(r, z, t) := (r \cos t, r \sin t, z)$, $r \geq 0$, $t \in [-\pi, \pi]$, $\Gamma := \left\{\mathbf{y}(p, t) \in \mathbb{R}^3 \; : \; p \in [0, 1], t \in [-\pi, \pi]\right\}$, $\mathbf{y}(p, t) := (r(p) \cos t, r(p) \sin t, z(p))$, $r(p) \geq 0$ for $p \in [0, 1]$, as well as axisymmetric current excitation $\mathbf{J}(\mathbf{x}(r, z, t)) := J(-\sin t, \cos t, 0)$ for $r \in [\underline{r}, \overline{r}]$, where $0 < \underline{r}$, $t \in [-\pi, \pi]$, $z \in [\underline{z}, \overline{z}]$, $\mathbf{J}(\mathbf{x}(r, z, t)) := \mathbf{0}$, elsewhere. Denoting $\boldsymbol{\varphi}(t) := (-\sin t, \cos t, 0)$, this gives rise to $\mathbf{u}(\mathbf{x}) =$

$u(r,z)\boldsymbol{\varphi}(t)$, $\mathbf{u}^{\rm e}(\mathbf{x}) = u^{\rm e}(r,z)\boldsymbol{\varphi}(t)$, $\boldsymbol{\lambda}(\mathbf{y}) = \lambda(p)\boldsymbol{\varphi}(t)$. The vectorial functions $\mathbf{u}(\mathbf{x})$, $\mathbf{v}(\mathbf{x})$, $\boldsymbol{\lambda}(\mathbf{y})$, $\boldsymbol{\xi}(\mathbf{y})$, and $\mathbf{J}(\mathbf{x})$ in (5) are respectively replaced by $u(r,z)$, $v(r,z)$, $\lambda(p)$, $\xi(p)$, and J, and the particular terms in (5) read as follows:

$$q(\mathbf{w};\mathbf{u},\mathbf{v}) = 2\pi \int_\omega dS(r,z)\, r\, \nu_{\rm r}\left(\left\|\widetilde{\mathbf{curl}}\, w(r,z)\right\|\right) \widetilde{\mathbf{curl}}\, u(r,z)\cdot \widetilde{\mathbf{curl}}\, v(r,z),$$

where $\widetilde{\mathbf{curl}}\, u(r,z) := \left(-\frac{\partial u(r,z)}{\partial z}, \frac{1}{r}\frac{\partial [u(r,z)r]}{\partial r}\right)$,

$$\langle \mathbf{N}(\boldsymbol{\gamma}_{\rm D}\mathbf{u}), \boldsymbol{\gamma}_{\rm D}\mathbf{v}\rangle_\Gamma = -\int_0^1 dp \int_0^1 ds \int_0^\pi d\alpha \left[\widetilde{\boldsymbol{\eta}}'(p)\cdot \widetilde{\mathbf{curl}}\, u(\boldsymbol{\eta}(p))\right] \times \left[\widetilde{\boldsymbol{\eta}}'(s)\cdot \widetilde{\mathbf{curl}}\, v(\boldsymbol{\eta}(s))\right] \frac{r(p)\, r(s)}{d(p,s,\alpha)^{1/2}},$$

where we denote $d(p,s,\alpha) := \|\boldsymbol{\eta}(p) - \boldsymbol{\eta}(s)\|^2 + 2r(p)\, r(s)(1-\cos\alpha)$, $\boldsymbol{\eta}(p) := (r(p), z(p))$ and $\widetilde{\boldsymbol{\eta}}(p) := (-z(p), r(p))$,

$$\langle \mathbf{B}(\boldsymbol{\lambda}), \boldsymbol{\gamma}_{\rm D}\mathbf{v}\rangle_\Gamma = -\pi \int_0^1 dp\, \lambda(p)\, v(\boldsymbol{\eta}(p))\, r(p)\, \|\boldsymbol{\eta}'(p)\| + \int_0^1 dp \int_0^1 ds \int_0^\pi d\alpha \frac{\lambda(p)\, v(\boldsymbol{\eta}(s))\, r(p)\, r(s)\, \|\boldsymbol{\eta}'(p)\|}{d(p,s,\alpha)^{3/2}}\, \widetilde{\boldsymbol{\eta}}'(s)\cdot \boldsymbol{\zeta}(p,s,\alpha)$$

where $\boldsymbol{\zeta}(p,s,\alpha) := (r(s)\cos\alpha - r(p), (z(s)-z(p))\cos\alpha)$,

$$\langle \boldsymbol{\xi}, \mathbf{A}(\boldsymbol{\lambda})\rangle_\Gamma = \int_0^1 dp \int_0^1 ds \int_0^\pi d\alpha \frac{\xi(s)\, \lambda(p)\, r(p)\, r(s)}{d(p,s,\alpha)^{1/2}}\, \|\boldsymbol{\eta}'(p)\|\, \|\boldsymbol{\eta}'(s)\|,$$

$$\langle \boldsymbol{\gamma}_{\rm N}^{\rm e}\mathbf{G}(\mathbf{J}/\nu_0), \boldsymbol{\gamma}_{\rm D}\mathbf{v}\rangle_\Gamma = \frac{J}{\nu_0}\int_0^1 ds \int_{\underline{r}}^{\overline{r}} dr \int_{\underline{z}}^{\overline{z}} dz \int_0^\pi d\alpha \frac{v(\boldsymbol{\eta}(s))\, r\, r(s)\, \widetilde{\boldsymbol{\eta}}'(s)\cdot \boldsymbol{\zeta}(r,z,s,\alpha)}{d(r,z,s,\alpha)^{3/2}}$$

where $d(r,z,s,\alpha) := \|(r,z) - \boldsymbol{\eta}(s)\|^2 + 2r\, r(s)(1-\cos\alpha)$ and $\boldsymbol{\zeta}(r,z,s,\alpha) := (r(s)\cos\alpha - r, (z(s)-z)\cos\alpha)$,

$$\langle \boldsymbol{\xi}, \boldsymbol{\gamma}_{\rm D}^{\rm e}\mathbf{G}(\mathbf{J}/\nu_0)\rangle_\Gamma \quad = \quad \frac{J}{\nu_0}\int_0^1 ds \int_{\underline{r}}^{\overline{r}} dr \int_{\underline{z}}^{\overline{z}} dz \int_0^\pi d\alpha \frac{\xi(s)\, r\, r(s)\, \|\boldsymbol{\eta}'(s)\|\, \cos\alpha}{d(r,z,s,\alpha)^{1/2}}.$$

Further, we need to evaluate the exterior magnetic flux density

$$\mathbf{B}^{\rm e} := \mathbf{curl}\, \mathbf{u}^{\rm e} = \mathbf{curl}\, \boldsymbol{\Psi}_{\rm M}\left(\boldsymbol{\gamma}_{\rm D}^{\rm e}\mathbf{u}^{\rm e}\right) - \mathbf{curl}\, \boldsymbol{\Psi}_{\rm A}\left(\boldsymbol{\lambda}\right) + \mathbf{curl}\, \mathbf{G}(\mathbf{J}/\nu_0), \qquad (8)$$

see (2), where the particular terms in the axisymmetric plane are as follows:

$$\mathbf{curl}\, \boldsymbol{\Psi}_{\rm M}\left(\boldsymbol{\gamma}_{\rm D}^{\rm e}\mathbf{u}^{\rm e}\right)(x_1,0,x_3) = \int_0^1 dp \int_0^\pi dt \frac{u(\boldsymbol{\eta}(p))\, r(p)}{2\pi\, d(x_1,x_3,p,t)^{3/2}} \times \left[(r'(p)\cos t, 0, z'(p)) + \frac{3e(x_1,x_3,p,t)}{d(x_1,x_3,p,t)}(x_3 - z(p), 0, -(x_1 - r(p)\cos t))\right],$$

where $e(x_1, x_3, p, t) := z'(p)(x_1 - r(p)\cos t) - r'(p)(x_3 - z(p))\cos t$,

$$\mathbf{curl}\,\boldsymbol{\Psi}_{\mathrm{A}}\,(\boldsymbol{\lambda})\,(x_1, 0, x_3) = \int_0^1 dp \int_0^\pi dt \frac{\lambda(p)\, r(p)\, \|(r'(p), z'(p))\|}{2\pi\, d(x_1, x_3, p, t)^{3/2}} \times ((x_3 - z(p))\cos t, 0, r(p) - x_1 \cos t),$$

$$\mathbf{curl}\,\mathbf{G}(\mathbf{J}/\nu_0)(x_1, 0, x_3) = \frac{J}{\nu_0} \int_{\underline{r}}^{\overline{r}} dr \int_{\underline{z}}^{\overline{z}} dz \int_0^\pi dt \frac{r\,((x_3 - z)\cos t, 0, r - x_1 \cos t)}{2\pi d(x_1, x_3, p, t)^{3/2}}.$$

It holds that $\mathbf{B}^{\mathrm{e}}(r\cos t, r\sin t, z) = (B_1^{\mathrm{e}}(r, 0, z)\cos t, B_1^{\mathrm{e}}(r, 0, z)\sin t, B_3^{\mathrm{e}}(r, 0, z))$.

Provided polygonal ω, our axisymmetric FEM–BEM method simplifies the original ansatz so that we only need to triangulate the axisymmetric domain $\omega = \bigcup_{i=1}^{t} \overline{T_i}$ with $T_i \cap T_j = \emptyset$ for $i \neq j$. Then, $\mathbf{V}_h := \langle \mathbf{v}_1, \ldots, \mathbf{v}_n \rangle$ becomes a space of first–order triangular FE–elements, and $\boldsymbol{\Lambda}_h := \langle \boldsymbol{\xi}_1, \ldots, \boldsymbol{\xi}_m \rangle$ becomes a space of piecewise constant functions along the segmentation of $\partial\omega = \bigcup_{i=1}^{m} \overline{S_i}$ with $S_i \cap S_j = \emptyset$ for $i \neq j$. This results in matrices $\boldsymbol{Q}(\boldsymbol{u}) := (q(\mathbf{u}; \mathbf{v}_i, \mathbf{v}_j))_{ij} \in \mathbb{R}^{n\times n}$, $\boldsymbol{N} := (\langle \mathbf{N}(\boldsymbol{\gamma}_{\mathrm{D}}\mathbf{v}_i), \boldsymbol{\gamma}_{\mathrm{D}}\mathbf{v}_j\rangle_\Gamma)_{ij} \in \mathbb{R}^{n\times n}$, $\boldsymbol{B} := (\langle \mathbf{B}(\boldsymbol{\xi}_i), \boldsymbol{\gamma}_{\mathrm{D}}\mathbf{v}_j\rangle_\Gamma)_{ij} \in \mathbb{R}^{n\times m}$, $\boldsymbol{A} := \big(\langle \boldsymbol{\xi}_i, \mathbf{A}(\boldsymbol{\xi}_j)\rangle_\Gamma\big)_{ij} \in \mathbb{R}^{m\times m}$, and the vectors $\boldsymbol{f} := (\langle \boldsymbol{\gamma}_{\mathrm{N}}^{\mathrm{e}}\mathbf{G}(\mathbf{J}/\nu_0), \boldsymbol{\gamma}_{\mathrm{D}}\mathbf{v}_i\rangle_\Gamma)_i \in \mathbb{R}^n$, $\boldsymbol{g} := (\langle \boldsymbol{\xi}_i, \boldsymbol{\gamma}_{\mathrm{D}}^{\mathrm{e}}\mathbf{G}(\mathbf{J}/\nu_0)\rangle_\Gamma)_i \in \mathbb{R}^m$. The resulting nonlinear block skew–symmetric system, related to (5),

$$\boldsymbol{\mathcal{A}}(\boldsymbol{u})(\boldsymbol{u}, \boldsymbol{l}) := \begin{pmatrix} \boldsymbol{Q}(\boldsymbol{u}) - \boldsymbol{N} & \boldsymbol{B} \\ -\boldsymbol{B}^T & \boldsymbol{A} \end{pmatrix} \begin{pmatrix} \boldsymbol{u} \\ \boldsymbol{l} \end{pmatrix} = \begin{pmatrix} \boldsymbol{f} \\ \boldsymbol{g} \end{pmatrix} =: \boldsymbol{\mathcal{B}} \tag{9}$$

is then solved by Algorithm 1, where $\boldsymbol{\mathcal{A}}'(\boldsymbol{u}^k)$ is the derivative of $\boldsymbol{\mathcal{A}}$ at $\boldsymbol{u}^k$. The solution is given by $\mathbf{u}^{\mathrm{e}}(\mathbf{x}) = \sum_{i=1}^{n} u_i \mathbf{v}_i(\mathbf{x})$ and $\boldsymbol{\lambda}(\mathbf{y}) = \sum_{i=1}^{m} l_i \boldsymbol{\xi}_i(\mathbf{y})$.

Algorithm 1 Damped Newton method for elimination of the state problem

Given a precision $\varepsilon > 0$
Solve $\boldsymbol{\mathcal{A}}(\mathbf{0})(\boldsymbol{u}^0, \boldsymbol{l}^0) = \boldsymbol{\mathcal{B}}$
$\boldsymbol{\mathcal{B}}^0 := \boldsymbol{\mathcal{B}} - \boldsymbol{\mathcal{A}}(\boldsymbol{u}^0)(\boldsymbol{u}^0, \boldsymbol{l}^0)$, $k := 0$
while $\|\boldsymbol{\mathcal{B}}^k\|/\|\boldsymbol{\mathcal{B}}\| > \varepsilon$ **do**
  Solve $\boldsymbol{\mathcal{A}}'(\boldsymbol{u}^k)(\boldsymbol{v}^k, \boldsymbol{m}^k) = \boldsymbol{\mathcal{B}}^k$
  Find $\tau^k > 0 : \|\boldsymbol{\mathcal{B}} - \boldsymbol{\mathcal{A}}(\boldsymbol{u}^k + \tau^k \boldsymbol{v}^k)(\boldsymbol{u}^k + \tau^k \boldsymbol{v}^k, \boldsymbol{\lambda}^k + \tau^k \boldsymbol{m}^k)\| < \|\boldsymbol{\mathcal{B}}^k\|$
  $(\boldsymbol{u}^{k+1}, \boldsymbol{l}^{k+1}) := (\boldsymbol{u}^k, \boldsymbol{l}^k) + \tau^k(\boldsymbol{v}^k, \boldsymbol{m}^k)$
  $\boldsymbol{\mathcal{B}}^{k+1} := \boldsymbol{\mathcal{B}} - \boldsymbol{\mathcal{A}}(\boldsymbol{u}^{k+1})(\boldsymbol{u}^{k+1}, \boldsymbol{l}^{k+1})$, $k := k + 1$
end while

2.3 Gaussian quadrature for the BEM integrals

Consider a local segment parameterization $S_i := \{\boldsymbol{\eta}_i(p) := (r_i(p), z_i(p)) \in \mathbb{R}^2 : p \in [0, 1]\}$ with $r_i(p) := a_i p + b_i$, $z_i(p) := c_i p + d_i$ for $i \in \{1, 2, \ldots, m\}$. The matrices $\boldsymbol{N}$, $\boldsymbol{B}$, and $\boldsymbol{A}$ are evaluated as sums over the following integrals:

$$\int_0^1 dp \int_0^1 ds \int_0^\pi d\alpha \, \frac{n^{(i,j)}(p, s, \alpha)}{d^{(i,j)}(p, s, \alpha)^{r/2}}, \quad r \in \{1, 3\}, \tag{10}$$

where the kernel, denoted by $k^{(i,j)}(p,s,\alpha) := n^{(i,j)}(p,s,\alpha)/d^{(i,j)}(p,s,\alpha)^{r/2}$, is Cauchy–singular whenever $\boldsymbol{\eta}_i(p) = \boldsymbol{\eta}_j(s)$ and $\alpha = 0$. We aim to apply a Gaussian quadrature after the following recipe of Sauter and Schwab [SS97, SS04]: introduce local coordinates, split the integration domain into simplices and then regularize the integrand via the Duffy transform [Duf82]. We distinguish three cases: identical segments, a common vertex, and distinct segments. Our analysis is only concerned with the worst situation, i.e. the second integral in $\boldsymbol{B}$, while the resulting integral regularizations apply to the cases of $\boldsymbol{N}$ and $\boldsymbol{A}$ too.

In case of identical panels the second integral in $\boldsymbol{B}$ reads as follows:

$$\int_0^1 dp \int_0^1 ds \int_0^\pi d\alpha \frac{f_1^{(i)}(p,s)(1-\cos\alpha)}{\sqrt{\left[(a_i^2+c_i^2)(p-s)^2 + 2f_2^{(i)}(p,s)(1-\cos\alpha)\right]^3}}, \tag{11}$$

where $f_1^{(i)}(p,s) := \xi v(s) c_i r_i(p)^2 r_i(s)\sqrt{a_i^2+c_i^2}$ with $v(s) := as+b$, $f_2^{(i)} := 2r_i(p)r_i(s)$. Let us introduce $z := p-s$, $\pi u := \alpha$ and denote the kernel in (11) by $\widetilde{k}^{(i)}(p,s,\alpha)$. Simple manipulations yield

$$\begin{aligned}\int_0^1 dp \int_0^1 ds \int_0^\pi d\alpha\, \widetilde{k}^{(i)}(p,s,\alpha) &= \pi \int_0^1 dp \int_{p-1}^p dz \int_0^1 du\, \widetilde{k}^{(i)}(p,p-z,\pi u) \\ &= \pi \int_0^1 dz \int_0^1 du \int_0^{1-z} dp \left(\widetilde{k}^{(i)}(p,p+z,\pi u) + \widetilde{k}^{(i)}(p+z,p,\pi u)\right).\end{aligned}$$

The latter integrand is singular at $z = u = 0$, which we treat via splitting the domain and the Duffy transforms $\tau := z$, $u =: \tau\eta$ and $\tau := u$, $z =: u\eta$, respectively, as follows:

$$\begin{aligned}&= \int_0^1 dz \int_0^z du \int_0^1 d\xi\, \widetilde{K}^{(i)}(\xi,z,u) + \int_0^1 du \int_0^u dz \int_0^1 d\xi\, \widetilde{K}^{(i)}(\xi,z,u) \\ &= \int_0^1 d\tau \int_0^1 d\eta \int_0^1 d\xi\, \tau\, K^{(i)}(\xi,\tau,\eta),\end{aligned} \tag{12}$$

where $\widetilde{K}^{(i)}(\xi,z,u) := \pi(1-z)\left(\widetilde{k}^{(i)}(p,p+z,\pi u) + \widetilde{k}^{(i)}(p+z,p,\pi u)\right)$ under the substitution $p =: (1-z)\xi$, and where $K^{(i)}(\xi,\tau,\eta) := \widetilde{K}^{(i)}(\xi,\tau,\tau\eta) + \widetilde{K}^{(i)}(\xi,\tau\eta,\tau)$. Now it is easy to see that both $\tau\,\widetilde{K}^{(i)}(\xi,\tau,\tau\eta)$ and $\tau\,\widetilde{K}^{(i)}(\xi,\tau\eta,\tau)$ are analytical in $[0,1]^3$ unless $r_i(0) = 0$ or $r_i(1) = 0$, while making use of

$$1-\cos\alpha = \alpha^2 \sum_{n=1}^{\infty} (-1)^{n+1} \frac{\alpha^{2(n-1)}}{(2n)!}, \quad \lim_{\alpha\to 0} \frac{1-\cos\alpha}{\alpha^2} = \frac{1}{2}. \tag{13}$$

Therefore, we are justified to use a tensor–product Gaussian quadrature applied to the second line of (12). It remains to consider the case of $r_i(p) = 0$ for $p \in \{0,1\}$ and $p = s$, i.e. contributions of segments with an end point at the r–axis. Then, the integrand in (11) has the following removable singularity: $(1-\cos\alpha)\lim_{p\to 0_+} f_1^{(i)}(p,p)/\sqrt{f_2^{(i)}(p,p)^3} = \xi v(p) c_i \sqrt{a_i^2+c_i^2}(1-\cos\alpha)/\sqrt{8}$.

In case of a common vertex $\mathbf{p} := \overline{S_i} \cap \overline{S_j}$ we assume $\mathbf{p} = \boldsymbol{\eta}_i(0) = \boldsymbol{\eta}_j(0)$, i.e. $b_i = b_j$ and $d_i = d_j$. The second integral in $\boldsymbol{B}$ reads as follows:

$$\int_0^1 dp \int_0^1 ds \int_0^\pi d\alpha \frac{f_1^{(i,j)}(p,s)\,[c_j r_i(p)(1-\cos\alpha) + (a_i c_j - a_j c_i) p \cos\alpha]}{\sqrt{\Big[(a_i p - a_j s)^2 + (c_i p - c_j s)^2 + 2 f_2^{(i,j)}(p,s)(1-\cos\alpha)\Big]^3}} \tag{14}$$

where $f_1^{(i,j)}(p,s) := \xi v(s) r_i(p) r_j(s) \sqrt{a_i^2 + c_i^2}$, and $f_2^{(i,j)} := 2 r_i(p) r_j(s)$. Let us introduce $\pi u := \alpha$, denote the kernel in (14) by $\widetilde{k}^{(i,j)}(p,s,\alpha) =: \frac{1}{\pi} k^{(i,j)}(p,s,u)$, which has a singularity at the origin. Following [Duf82], we split the domain into three pyramids and use the transform $s =: p\eta$, $u =: p\tau$ as follows:

$$\begin{aligned} &= \int_0^1 dp \int_0^p ds \int_0^p du\, k^{(i,j)}(p,s,u) + \int_0^1 ds \int_0^s du \int_0^s dp\, k^{(i,j)}(p,s,u) \\ &\quad + \int_0^1 du \int_0^u dp \int_0^u ds\, k^{(i,j)}(p,s,u) = \int_0^1 dp \int_0^p ds \int_0^p du\, K^{(i,j)}(p,s,u) \qquad (15) \\ &= \int_0^1 dp \int_0^1 d\eta \int_0^1 d\tau\, p^2 K^{(i,j)}(p, p\eta, p\tau), \end{aligned}$$

where $K^{(i,j)}(p,s,u) := k^{(i,j)}(p,s,u) + k^{(i,j)}(s,u,p) + k^{(i,j)}(u,p,s)$. It is again easy to see that $p^2 K^{(i,j)}(p, p\eta, p\tau)$ is analytic in $[0,1]^3$, while making use of (13). Therefore, we can apply a tensor–product Gaussian quadrature to the second line of (15). There is no other singularity provided Lipschitz continuity of Ω.

Finally, in case of distinct segments, the integrand in (14) is analytical in $[0,1]^2 \times [0,\pi]$ and we can directly apply a Gaussian quadrature.

3 Shape optimization problem

Given a compact set of functions controlling the boundary Γ, denote the α–dependent solution to (5) by $(\mathbf{u}(\alpha), \boldsymbol{\lambda}(\alpha))$ and denote by $\mathbf{B}^{\mathrm{e}}(\mathbf{u}, \boldsymbol{\lambda})$ the related exterior magnetic flux density (8) in $\Theta := \Omega^{\mathrm{m}} \cup \Omega^{\mathrm{o}} \subset \Omega^{\mathrm{e}}$, see Fig. 1. Further, we denote by $\mathcal{I} : \big[L^2(\Theta)\big]^3 \to \mathbb{R}$ and $\mathcal{C} : \big[L^2(\Theta)\big]^3 \to \mathbb{R}$ a nonlinear objective and constraint functional, respectively. The abstract shape optimization problem under consideration reads as follows:

$$\min_{\alpha \in \mathcal{U}} \mathcal{I}(\mathbf{B}^{\mathrm{e}}(\mathbf{u}(\alpha), \boldsymbol{\lambda}(\alpha))) \quad \text{subject to (5) and } \mathcal{C}(\mathbf{B}^{\mathrm{e}}(\mathbf{u}(\alpha), \boldsymbol{\lambda}(\alpha))) \le 0. \tag{16}$$

The problem (16) is approximated by

$$\min_{\boldsymbol{p} \in \mathcal{P}} \mathcal{J}(\boldsymbol{p}) \quad \text{subject to (9) and } \mathcal{D}(\boldsymbol{p}) \le 0, \tag{17}$$

where $\boldsymbol{p}$ is a vector of Bézier parameters, which control the boundary Γ as well as the discretized state problem (9), $\mathcal{P} := \{\boldsymbol{p} \in \mathbb{R}^d : \boldsymbol{P}\boldsymbol{p} \le \boldsymbol{q}\}$, $\boldsymbol{P} \in \mathbb{R}^{e \times d}$, $\boldsymbol{q} \in \mathbb{R}^e$, where further $F : \mathcal{P} \to \mathcal{U}$ denotes the Bézier parameterization, and where $\mathcal{J}(\boldsymbol{p}) := \mathcal{I}(\mathbf{B}^{\mathrm{e}}(\mathbf{u}(F(\boldsymbol{p})), \boldsymbol{\lambda}(F(\boldsymbol{p}))))$ and $\mathcal{D}(\boldsymbol{p}) := \mathcal{C}(\mathbf{B}^{\mathrm{e}}(\mathbf{u}(F(\boldsymbol{p})), \boldsymbol{\lambda}(F(\boldsymbol{p}))))$.

There is yet another subproblem to solve, which is a deformation of the triangulation of ω with respect to the shape perturbation $\alpha := F(\boldsymbol{p})$. This we formulate as an auxiliary 2–dimensional torsion–free linear elasticity problem with the nonhomogeneous boundary Dirichlet displacement $F(\boldsymbol{p})$ along Γ, which is prescribed via a penalty $\rho \gg 0$. The problem is as follows: find nodal grid displacements $\boldsymbol{z} \in \mathbb{R}^{2n}$ such that

$$(\boldsymbol{K} + \rho \boldsymbol{K}_\Gamma)\, \boldsymbol{z} = \rho \boldsymbol{K}_\Gamma\, \boldsymbol{F}(\boldsymbol{p}), \tag{18}$$

where $\boldsymbol{K} \in \mathbb{R}^{2n \times 2n}$ is the discretized tensor–product Laplacian, $\boldsymbol{K}_\Gamma \in \mathbb{R}^{2n \times 2n}$ is the boundary mass matrix along Γ, and $\boldsymbol{F} : \mathbb{R}^d \to \mathbb{R}^{2(m+1)}$ is a vector counterpart of discretized F, which computes shape displacements of the $m+1$ nodes along Γ by means of the Bézier parameterization.

Denote by $\boldsymbol{I}, \boldsymbol{C} : \mathbb{R}^{2\theta} \to \mathbb{R}$ the vector counterparts of discretized $\mathcal{I}$ and $\mathcal{C}$, respectively, and by $\boldsymbol{B}^{\mathrm{e}} \in \mathbb{R}^{2\theta}$ the vector of the exterior magnetic flux components $(B_1^{\mathrm{e}}(r,0,z), B_3^{\mathrm{e}}(r,0,z))$ at θ points $(r,0,z) \in \Theta$, computed by means of (8). Altogether, the evaluation of $\mathcal{J}(\boldsymbol{p})$ and $\mathcal{D}(\boldsymbol{p})$ performs as follows:

$$\begin{array}{ccccccc}
\boldsymbol{p} & \xrightarrow{\boldsymbol{F}} & \boldsymbol{\alpha} & \xrightarrow{(18)} & \boldsymbol{z} & \xrightarrow[\text{Gauss quadrature}]{\text{FEM/BEM assembling}} & \boldsymbol{\mathcal{A}}, \boldsymbol{\mathcal{B}} \\
 & & & & \downarrow & & \text{Alg. 1} \downarrow (9) \\
\mathcal{J}(\boldsymbol{p}), \mathcal{D}(\boldsymbol{p}) & \xleftarrow{\boldsymbol{I}, \boldsymbol{C}} & & & \boldsymbol{B}^{\mathrm{e}} & \xleftarrow[\text{Gauss quadrature}]{\text{assembling by (8)}} & \boldsymbol{u}, \boldsymbol{l}
\end{array} \tag{19}$$

3.1 Optimization method

We aim to solve the discretized problem (17) using a gradient–type algorithm, which additionaly assumes $\mathcal{J}$ and $\mathcal{D}$ to be continuously differentiable. To this end we first introduce a fast projection onto a cone of linear constraints. Given a feasible $\boldsymbol{p}^k$, i.e. $\boldsymbol{p}^k \in \mathcal{P} : \mathcal{D}(\boldsymbol{p}^k) \le 0$, denote $\mathcal{J}^k := \mathcal{J}(\boldsymbol{p}^k)$, $\boldsymbol{g}^k := \nabla \mathcal{J}(\boldsymbol{p}^k)$, $\mathcal{D}^k := \mathcal{D}(\boldsymbol{p}^k)$, $\boldsymbol{g}_{\mathrm{c}}^k := \nabla \mathcal{D}(\boldsymbol{p}^k)$. We denote the cone of linearized inequality constrains by

$$\mathcal{P}_{\mathrm{c}}^k := \left\{ \boldsymbol{p} \in \mathbb{R}^d \;:\; \boldsymbol{P}_{\mathrm{c}}^k \boldsymbol{p} \le \boldsymbol{q}_{\mathrm{c}}^k \right\}, \text{ where } \boldsymbol{P}_{\mathrm{c}}^k := \begin{pmatrix} \boldsymbol{P} \\ \boldsymbol{g}_{\mathrm{c}}^k \end{pmatrix} \text{ and } \boldsymbol{q}_{\mathrm{c}}^k := \begin{pmatrix} \boldsymbol{q} \\ \boldsymbol{g}_{\mathrm{c}}^k \cdot \boldsymbol{p}^k - \mathcal{D}^k \end{pmatrix}. \tag{20}$$

For $i \in \{1, 2, \ldots, e+1\}$ denote by $\left(\boldsymbol{P}_{\mathrm{c}}^k\right)_i$ and $\left(\boldsymbol{q}_{\mathrm{c}}^k\right)_i$ the i–th row of $\boldsymbol{P}_{\mathrm{c}}^k$ and the i–th component of $\boldsymbol{q}_{\mathrm{c}}^k$, respectively. Similarly, for $A \subset \{1, 2, \ldots, e+1\}$ we denote by $\left(\boldsymbol{P}_{\mathrm{c}}^k\right)_A$ and $\left(\boldsymbol{q}_{\mathrm{c}}^k\right)_A$ the related submatrix and subvector, respectively. By $(\boldsymbol{M}\boldsymbol{M}^T)^+$ we denote a pseudoinverse to the normal equation matrix $\boldsymbol{M}\boldsymbol{M}^T$. Provided e be small, for $\alpha > 0$, we employ Algorithm 2 to cheaply compute the Euclidean projection of a steepest descent step $\boldsymbol{p}^k - \alpha \boldsymbol{g}^k$ onto $\mathcal{P}_{\mathrm{c}}^k$. The algorithm successively adds violated constraints into an active set and projects $\boldsymbol{p}^k - \alpha \boldsymbol{g}^k$ onto them. It stops after at most $e+1$ iterations.

Algorithm 2 Projection onto $\mathcal{P}_{\mathrm{c}}^k$

Given a feasible design $\boldsymbol{p}^k$, a step size $\alpha > 0$, the direction $\boldsymbol{g}^k$, and $\mathcal{P}_{\mathrm{c}}^k$ by (20)
$A := \emptyset$, $I := \{1, 2, \ldots, e+1\}$, $\tilde{\boldsymbol{p}}^k := \boldsymbol{p}^k$, $\tilde{\boldsymbol{p}}^{k+1} := \boldsymbol{p}^k - \alpha \boldsymbol{g}^k$
while $\exists i \in I : \left(\boldsymbol{P}_{\mathrm{c}}^k\right)_i \cdot \tilde{\boldsymbol{p}}^{k+1} > (\boldsymbol{q}_{\mathrm{c}}^k)_i$ **do**
$\widetilde{A} := \left\{ i \in I : \left(\boldsymbol{P}_{\mathrm{c}}^k\right)_i \cdot \tilde{\boldsymbol{p}}^{k+1} > (\boldsymbol{q}_{\mathrm{c}}^k)_i \right\}$
$(\widetilde{\alpha}, i) := \min\limits_{i \in \widetilde{A}} \left[\left(\boldsymbol{q}_{\mathrm{c}}^k\right)_i - \left(\boldsymbol{P}_{\mathrm{c}}^k\right)_i \cdot \tilde{\boldsymbol{p}}^k \right] / \left[\left(\boldsymbol{P}_{\mathrm{c}}^k\right)_i \cdot (\tilde{\boldsymbol{p}}^{k+1} - \tilde{\boldsymbol{p}}^k) \right]$
$A := A \cup \{i\}$, $I := I \setminus \{i\}$, $\boldsymbol{M} := \left(\boldsymbol{P}_{\mathrm{c}}^k\right)_A$, $\boldsymbol{v} := \left(\boldsymbol{q}_{\mathrm{c}}^k\right)_A$
$\tilde{\boldsymbol{p}}^k := \tilde{\boldsymbol{p}}^k + \widetilde{\alpha}(\tilde{\boldsymbol{p}}^{k+1} - \tilde{\boldsymbol{p}}^k)$
$\tilde{\boldsymbol{p}}^{k+1} := \boldsymbol{p}^k - \alpha \boldsymbol{g}^k$
$\tilde{\boldsymbol{p}}^{k+1} := \tilde{\boldsymbol{p}}^{k+1} + \boldsymbol{M}^T (\boldsymbol{M}\boldsymbol{M}^T)^+ (\boldsymbol{v} - \boldsymbol{M}\tilde{\boldsymbol{p}}^{k+1})$
end while
$\boldsymbol{p}^{k+1} := \tilde{\boldsymbol{p}}^{k+1}$ is the resulting projection

To solve (17), we now employ Algorithm 3, which is based on the steepest–descent search, an active–set approach, and a trust–region modification of the step size α.

Algorithm 3 Steepest–descent active–set optimization method

Given a feasible design $\boldsymbol{p}^0$ and precisions $\varepsilon_1, \varepsilon_2 > 0$
$\alpha := 1$, $k := 0$
Compute $\mathcal{J}^k$, $\boldsymbol{g}^k$, $\mathcal{D}^k$, and $\boldsymbol{g}_c^k$
Project $\boldsymbol{p}^0 - \boldsymbol{g}^0$ onto $\mathcal{P}_{\mathrm{c}}^0$ using Algorithm 2 $\rightsquigarrow \tilde{\boldsymbol{p}}^0$
$\boldsymbol{g}_{\mathrm{feas}}^0 := \boldsymbol{p}^0 - \tilde{\boldsymbol{p}}^0$
while $k = 0$ or $(\|\boldsymbol{g}_{\mathrm{feas}}^k\| / \|\boldsymbol{g}_{\mathrm{feas}}^0\| > \varepsilon_1$ and $|\mathcal{J}^k - \mathcal{J}^{k-1}| / |\mathcal{J}^0| > \varepsilon_2)$ **do**
repeat
Project $\boldsymbol{p}^k - \alpha \boldsymbol{g}^k$ onto $\mathcal{P}_{\mathrm{c}}^k$ using Algorithm 2 $\rightsquigarrow \boldsymbol{p}^{k+1}$
Compute $\mathcal{J}^{k+1}$ and $\mathcal{D}^{k+1}$
$\alpha := \alpha / 2$
until $\mathcal{J}^{k+1} < \mathcal{J}^k$ and $\mathcal{D}^{k+1} \leq 0$
Compute $\boldsymbol{g}^{k+1}$ and $\boldsymbol{g}_c^{k+1}$
Project $\boldsymbol{p}^{k+1} - \boldsymbol{g}^{k+1}$ onto $\mathcal{P}_{\mathrm{c}}^{k+1}$ using Algorithm 2 $\rightsquigarrow \tilde{\boldsymbol{p}}^{k+1}$
$\boldsymbol{g}_{\mathrm{feas}}^{k+1} := \boldsymbol{p}^{k+1} - \tilde{\boldsymbol{p}}^{k+1}$
$\alpha := 2\alpha$, $k := k + 1$
end while

3.2 Shape sensitivity analysis

Yet, we have to efficiently compute $\boldsymbol{g}^k$ and $\boldsymbol{g}_{\mathrm{c}}^k$ by differentiating the compound map (19) by means of the adjoint method of semi–analytical sensitivity analysis, cf. [HCK86], which is based on a solution to an adjoint equation of (9).

In (19) the only nontrivial map to differentiate is (9), solved by Algorithm 1. We can do a backward differentiation of Algorithm 1, as we proposed in [LC07], which is however rather technical from the implemetation point of view. Rather, at the iteration $(\boldsymbol{u}^k, \boldsymbol{l}^k)$ we consider an approximation of the original nonlinear state problem (9) by the linear counterpart

$$\boldsymbol{\mathcal{A}}(\boldsymbol{z}^k, \boldsymbol{u}^k)(\boldsymbol{u}, \boldsymbol{l}) = \boldsymbol{\mathcal{B}}(\boldsymbol{z}^k), \tag{21}$$

where we additionaly express the dependence on the displaced grid nodes $\boldsymbol{z}^k$. In order to apply the adjoint method we only need derivatives of $\boldsymbol{\mathcal{A}}(\boldsymbol{z}^k, \boldsymbol{u}^k)$ and $\boldsymbol{\mathcal{B}}(\boldsymbol{z}^k)$ with respect to the nodal displacements $\boldsymbol{z}^k$ in a direction $\boldsymbol{\vartheta} \in \mathbb{R}^{2n}$, which we denote by $\nabla_{\boldsymbol{z}} \boldsymbol{\mathcal{A}}(\boldsymbol{z}^k, \boldsymbol{u}^k) \cdot \boldsymbol{\vartheta}$ and $\nabla_{\boldsymbol{z}} \boldsymbol{\mathcal{B}}(\boldsymbol{z}^k) \cdot \boldsymbol{\vartheta}$, respectively. Referring to Sec. 2.3, we can see that all the contributions to both $\boldsymbol{\mathcal{A}}(\boldsymbol{z}^k, \boldsymbol{u}^k)$ and $\boldsymbol{\mathcal{B}}(\boldsymbol{z}^k)$ have the following form:

$$\sum_{i_1=1}^{n_1^{\mathrm{G}}} w_{i_1}^{\mathrm{G},n_1^{\mathrm{G}}} \cdots \sum_{i_j=1}^{n_j^{\mathrm{G}}} w_{i_j}^{\mathrm{G},n_j^{\mathrm{G}}} f\left(\boldsymbol{z}^k, \boldsymbol{u}^k, x_{i_1}^{\mathrm{G},n_1^{\mathrm{G}}}, \ldots, x_{i_j}^{\mathrm{G},n_j^{\mathrm{G}}}\right),$$

where f is the regularized integrand, j is the number of involved segment integrals, n^{G} denotes the order of Gaussian quadrature, and, for $i \in \{1, 2, \ldots, n^{\mathrm{G}}\}$, $w_i^{\mathrm{G},n^{\mathrm{G}}} \in \mathbb{R}$ and $x_i^{\mathrm{G},n^{\mathrm{G}}} \in (0,1)$ denote the related Gauss quadrature weights and points, respectively. Thus, the directional derivatives are assembled out of contributions of the following type:

$$\sum_{l=1}^{2n} \sum_{i_1=1}^{n_1^{\mathrm{G}}} w_{i_1}^{\mathrm{G},n_1^{\mathrm{G}}} \cdots \sum_{i_j=1}^{n_j^{\mathrm{G}}} w_{i_j}^{\mathrm{G},n_j^{\mathrm{G}}} \frac{\partial f\left(\boldsymbol{z}^k, \boldsymbol{u}^k, x_{i_1}^{\mathrm{G},n_1^{\mathrm{G}}}, \ldots, x_{i_j}^{\mathrm{G},n_j^{\mathrm{G}}}\right)}{\partial z_l} \vartheta_l,$$

which are certainly evaluated only for l related to the finite or boundary element under consideration. A similar technique applies to $\nabla_{\boldsymbol{z}} \boldsymbol{B}^{\mathrm{e}}(\boldsymbol{z}^k, \boldsymbol{u}^k, \boldsymbol{l}^k) \cdot \boldsymbol{\omega}_{\boldsymbol{z}}$, where $\boldsymbol{\omega}_{\boldsymbol{z}} \in \mathbb{R}^{2\theta}$ and the function $\boldsymbol{B}^{\mathrm{e}}$ is computed via (8) and Gaussian quadrature.

Altogether, evaluation of the shape derivatives $\boldsymbol{g}^k$ and $\boldsymbol{g}_{\mathrm{c}}^k$ is described in Algorithm 4. There, going backward through (19), we successively compute directional derivatives of $\boldsymbol{I}$ and $\boldsymbol{C}$, all denoted by symbols $\boldsymbol{\omega}$, with respect to $\boldsymbol{B}^{\mathrm{e}}$, $\boldsymbol{u}$, $\boldsymbol{l}$, $\boldsymbol{z}$, $\boldsymbol{\alpha}$, and $\boldsymbol{p}$. In the algorithm we adjoint the linear counterpart of the state equation (21) as well as the auxiliary elasticity shape–to–mesh map (18).

4 Numerical results

We consider the geometry of an electromagnet depicted in Fig. 1 (left). The nonlinear ferromagnetic reluctivity $\nu_{\mathrm{r}}(t)$ is depicted in Fig. 1 (right) such that $\nu_{\mathrm{r}}(B)\, B = H$. The function $\nu_{\mathrm{r}}(t)$ approximately models a measured B–H curve for the used kind of steel called AREMA so that it is twice continuously differentiable and it successively consists of 4 parts: a straight line from the origin up to $(B_0, H_0) := (1.25\,\mathrm{T}, 600\,\mathrm{A\,m^{-1}})$, two piece–wise cubic Bézier splines up

Algorithm 4 Adjoint shape sensitivity analysis

Given $\boldsymbol{p}^k \in \mathbb{R}^d$, $\boldsymbol{\alpha}^k \in \mathbb{R}^{2(m+1)}$, $\boldsymbol{z}^k \in \mathbb{R}^{2n}$, $\boldsymbol{u}^k \in \mathbb{R}^n$, $\boldsymbol{l}^k \in \mathbb{R}^m$, and $\boldsymbol{B}^{\mathrm{e}k} \in \mathbb{R}^{2\theta}$
$\boldsymbol{\omega}_{I,B^{\mathrm{e}}} := \nabla_{B^{\mathrm{e}}} \boldsymbol{I}(\boldsymbol{B}^{\mathrm{e}k})$ and $\boldsymbol{\omega}_{C,B^{\mathrm{e}}} := \nabla_{B^{\mathrm{e}}} \boldsymbol{C}(\boldsymbol{B}^{\mathrm{e}k})$
$(\boldsymbol{\omega}_{I,z}, \boldsymbol{\omega}_{C,z}) := \nabla_z \boldsymbol{B}^{\mathrm{e}}(\boldsymbol{z}^k, \boldsymbol{u}^k, \boldsymbol{l}^k) \cdot (\boldsymbol{\omega}_{I,B^{\mathrm{e}}}, \boldsymbol{\omega}_{C,B^{\mathrm{e}}})$
$(\boldsymbol{\omega}_{I,u}, \boldsymbol{\omega}_{C,u}) := \nabla_u \boldsymbol{B}^{\mathrm{e}}(\boldsymbol{z}^k, \boldsymbol{u}^k, \boldsymbol{l}^k) \cdot (\boldsymbol{\omega}_{I,B^{\mathrm{e}}}, \boldsymbol{\omega}_{C,B^{\mathrm{e}}})$
$(\boldsymbol{\omega}_{I,l}, \boldsymbol{\omega}_{C,l}) := \nabla_l \boldsymbol{B}^{\mathrm{e}}(\boldsymbol{z}^k, \boldsymbol{u}^k, \boldsymbol{l}^k) \cdot (\boldsymbol{\omega}_{I,B^{\mathrm{e}}}, \boldsymbol{\omega}_{C,B^{\mathrm{e}}})$
Solve $\boldsymbol{\mathcal{A}}(\boldsymbol{z}^k, \boldsymbol{u}^k)^T \cdot (\boldsymbol{\vartheta}_I, \boldsymbol{\vartheta}_C) = \begin{pmatrix} \boldsymbol{\omega}_{I,u} & \boldsymbol{\omega}_{C,u} \\ \boldsymbol{\omega}_{I,l} & \boldsymbol{\omega}_{C,l} \end{pmatrix}$
$(\boldsymbol{\omega}_{I,z}, \boldsymbol{\omega}_{C,z}) := (\boldsymbol{\omega}_{I,z}, \boldsymbol{\omega}_{C,z}) + \left[\nabla_z \boldsymbol{\mathcal{B}}(\boldsymbol{z}^k) - \nabla_z \boldsymbol{\mathcal{A}}(\boldsymbol{z}^k, \boldsymbol{u}^k)(\boldsymbol{u}, \boldsymbol{l})\right] \cdot (\boldsymbol{\vartheta}_I, \boldsymbol{\vartheta}_C)$
Solve $(\boldsymbol{K} + \rho \boldsymbol{K}_\Gamma)^T \cdot (\boldsymbol{\eta}_I, \boldsymbol{\eta}_C) = (\boldsymbol{\omega}_{I,z}, \boldsymbol{\omega}_{C,z})$
$(\boldsymbol{\omega}_{I,\alpha}, \boldsymbol{\omega}_{C,\alpha}) := (\rho \boldsymbol{K}_\Gamma)^T \cdot (\boldsymbol{\eta}_I, \boldsymbol{\eta}_C)$
The result is $\left(\boldsymbol{g}^k, \boldsymbol{g}_{\mathrm{c}}^k\right) := \nabla_p \boldsymbol{F}(\boldsymbol{p}^k) \cdot (\boldsymbol{\omega}_{I,\alpha}, \boldsymbol{\omega}_{C,\alpha})$

to $(B_1, H_1) := (1.625\,\mathrm{T}, 4\,\mathrm{kA\,m^{-1}})$ and $(B_2, H_2) := (1.75\,\mathrm{T}, 10\,\mathrm{kA\,m^{-1}})$, respectively, and $\nu_{\mathrm{r}}(t) := \nu_0 + c_1/t + c_2/t^2 + c_3/t^3$ for $t > B_2$, where recall that ν_0 denotes the air reluctivity. Further, we consider the current 1 A and the wire diameter 0.8 mm, which implies the current density $J := 1/(0.8\,10^{-3})^2\,\mathrm{A\,m^{-2}}$. There are 3281 turns around the pole head coil.

The optimization aims at developing a shape of the electromagnet core so that the resulting device is well–suited for measurements of magnetooptic effects on samples placed in the domain Ω^{m}, which is a cylinder of the radius 4 mm and the height 6 mm axisymmetrically placed 2 mm above the pole head. To this end, one wishes to maximize the average axial magnetic flux component in Ω^{m}, and, at the same time, to minimize a homogeneity, which we prescribe as the variance of the magnetic flux density in Ω^{m} by means of the minimal variance of the axial components from the average and the radial component from zero. It turns out that these two criterions are in a contrast. From our experience, we find reasonable to solve the two related optimization subproblems separately. First, we start from the design depicted in Fig. 1 (left) and minimize the variance

$$\kappa^2 := \frac{1}{|\Omega^{\mathrm{m}}|\,|B^{\mathrm{avg}}|^2} \int_{\Omega^{\mathrm{m}}} dV(r,z,t) \left[\left(B_1^{\mathrm{e}}(r,0,z)\right)^2 + \left(B_3^{\mathrm{e}}(r,0,z) - B^{\mathrm{avg}}\right)^2 \right],$$

where $|\Omega^{\mathrm{m}}|$ denotes the volume of Ω^{m} and where

$$B^{\mathrm{avg}} := \frac{1}{|\Omega^{\mathrm{m}}|} \int_{\Omega^{\mathrm{m}}} dV(r,z,t)\, B_3^{\mathrm{e}}(r,0,z).$$

Then, we prescribe a nonlinear constraint function $\mathcal{D} := \kappa^2 - (\kappa^{\mathrm{req}})^2$, where $\kappa^{\mathrm{req}} := 0.06$ is chosen by experience, and we maximize B^{avg} subject to $\mathcal{D} \le 0$, while starting from the design resulting from the previous minimization. In either case the optimization variables are axial coordinates of control nodes of three Bézier curves that respectively control the shapes of the pole head and of the bottom and top cover part, see Fig. 1 (left). We additionally prescribe

problem, n	optim. iters. (stopping)	Newton iters. (typical)	evolution of κ [%]	evolution of B^{avg} [T]
$\min \kappa$, 262	54 (ε_1)	5–13 (5)	2.6 $\rightarrow$ 0.5	0.153 $\rightarrow$ 0.119
$\max B^{\mathrm{avg}}$, 262	5 (ε_2)	5–13 (8)	0.5 $\rightarrow$ 6	0.119 $\rightarrow$ 0.231
$\min \kappa$, 902	35 (ε_1)	7–14 (7)	2.7 $\rightarrow$ 0.5	0.150 $\rightarrow$ 0.116
$\max B^{\mathrm{avg}}$, 902	15 (ε_2)	7–19 (12)	0.5 $\rightarrow$ 6	0.116 $\rightarrow$ 0.216

Table 1: Numerical results

geometrical nonpenetrating constraints as linear inequalities involved in $\boldsymbol{P}$ and $\boldsymbol{q}$, that preserve the Bézier control polygons from intersection.

In our numerical simulations there are $d := 16$ design variables: 3 along the pole head, 6 on the top cover, 6 on the bottom cover and 1 controlling the axial slope of the cover front, see Fig. 1 (left). In all cases the cover front turns out to be optimal parallel to the axis. We solve the optimization for two discretizations, both of which lead to same results. In particular, the FEM/BEM discretizations consist of $n := 262$ inner nodes and $m := 125$ boundary segments, and of $n := 902$ inner nodes and $m := 250$ boundary segments, respectively. All the involved BEM integrals are evaluated using the tensor–product Gaussian quadrature, see Sec. 2.3, with $n^{\mathrm{G}} := 6$ nodes in each direction. The relative precision for the damped Newton iterations, see Alg. 1, is $\varepsilon := 10^{-6}$ and the ones for the steepest–descent optimization, see Alg. 3, are $\varepsilon_1 := 10^{-3}$ and $\varepsilon_2 := 10^{-6}$. The penalty parameter for the elasticity map is $\rho := 10^6$. All the arising linear systems are solved by the Gaussian elimination. In order to evaluate κ^2 and B^{avg} approximately, the exterior magnetic flux density $(B_1^{\mathrm{e}}(r,0,z), B_3^{\mathrm{e}}(r,0,z))$ is computed on a cartesian grid over Ω^{m} consisting of 2 radial and 4 axial nodes.

Numerical simulations were done in MATLAB. The resulting shapes and magnetic fields are depicted in Fig. 2. The parameters of the optimization runs are summarized in Table 4. While within the minimization of κ we achieved a converge of the projected gradient, it was not the case for the successive maximization of B^{avg}, which escaped due to a small step size and no improvement of the cost functional. The reason might be that in the final stage of optimization the state sensitivity analysis of (21) is not a precise enough approximation. From the third column we can see a stability of Newton iterations. The last two columns document that the two optimization criterions go again each other.

References

[Beb00] Bebendorf, M.: Approximation of boundary element matrices. Numer. Math. **86**, 565–589 (2000)

[BC01a] Buffa, A., Ciarlet, P.: On traces for functional spaces related to Maxwell's equations. Part I: An integration by parts formula in Lipschitz polyhedra. Math. Meth. Appl. Sci. **24**, 9–30 (2001)

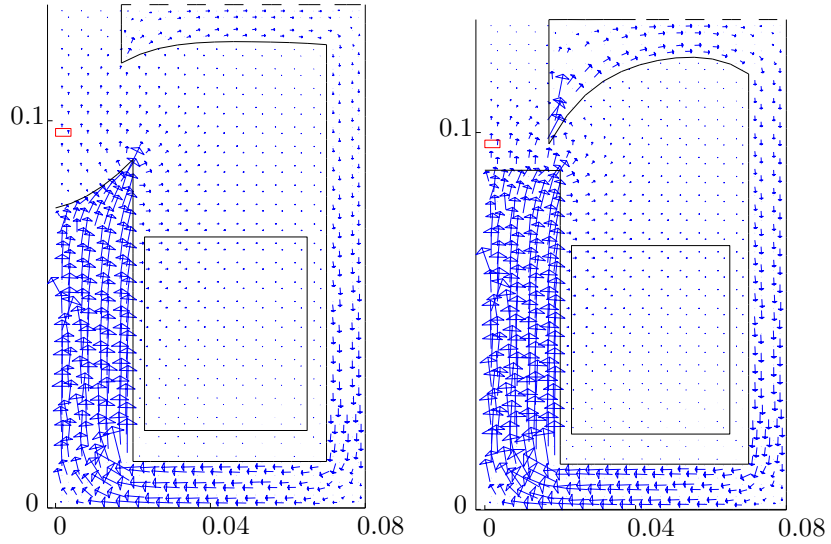

Figure 2: Resulting shapes (size in meters) and magnetic fields of minimization of κ^2 (left) and maximization of B^{avg} s.t. $\kappa \leq \kappa^{\text{req}}$ (right)

[BC01b] Buffa, A., Ciarlet, P.: On traces for functional spaces related to Maxwell's equations. Part II: Hodge decompositions on the boundary of Lipschitz polyhedra and applications. Math. Meth. Appl. Sci. **24**, 31–48 (2001)

[Cos87] Costabel, M.: Symmetric methods for the coupling of finite and boundary elements. In Boundary Elements IX, C. Brebbia, W. Wendland, and G. Kuhn (eds.), Springer–Verlag, Berlin, 411–420 (1987)

[Duf82] Duffy, M.G.: Quadrature over a pyramid or cube of integrands with a singularity at a vertex. SIAM J. Numer. Anal. **19**, 1260–1262 (1982)

[Epp00] Eppler, K.: Second detivatives and sufficient optimality conditions for shape functionals. Control and Cybernetics **29**, 485–512 (2000)

[EH06] Eppler, K., Harbrecht, H.: Second–order shape optimization using wavelet BEM. Optim. Methods Softw. **21**, 135–153 (2006)

[HN89] Hackbusch, W., Nowak, Z.P.: On the fast matrix multiplication in the boundary element methods by panel clustering. Numer. Math. **54**, 463–491 (1989)

[HN97] Haslinger, J., Neittaanmäki, P.: Finite Element Approximation for Optimal Shape, Material and Topology Design. Wiley, Chinchester (1997)

[Hip02] Hiptmair, R.: Symmetric coupling for eddy current problems. SIAM J. Numer. Anal. **40**, 41-65 (2002)

[HS98] Hubert, A., Schäfer, R.: Magnetic Domains: The Analysis of Magnetic Microstructures. Springer, Berlin (1998)

[HCK86] Haug, E.J., Choi, K.K., Komkov, V.: Sensitivity Analysis in Structural Design. Academic Press (1986)

[KS02] Kuhn, M., Steinbach, O.: Symmetric coupling of finite and boundary elements for exterior magnetic field problems. Math. Methods. Appl. Sci. **25**, 357–371 (2002)

[LC07] Lukáš, D., Chalmovianský, P.: A sequential coupling of optimal topology and multilevel shape design applied to 2–dimensional nonlinear magnetostatics. Comp. Vis. Sci. **10**, 135–144 (2007)

[Nec83] Nečas, J.: Introduction to the Theory of Nonlinear Elliptic Equations. B.G. Teubner, Leipzig (1983)

[Ned80] Nédélec, J.–C.: Mixed finite elements in $\mathbb{R}^3$. Numer. Math. **35**, 315–341 (1980)

[Pec04] Pechstein, C.: Multigrid–Newton Methods for Nonlinear Magnetostatic Problems. Master thesis. Johannes Kepler University Linz, Austria (2004)

[Pos02] Postava, K., Hrabovský, D., Pištora, J., Fert, A.R., Višňovský, Š., Yamaguchi, T.: Anisotropy of quadratic magneto-optic effects in reflection. J. Appl. Phys. **91**, 7293–7295 (2002)

[RS07] Steinbach, O., Rjasanow, S.: The Fast Solution of Boundary Integral Equations. Springer (2007)

[Rok85] Rokhlin, V.: Rapid solution of integral equations of classical potential theory. J. Comput. Phys. **60**, 187–207 (1985)

[SS97] Sauter, S., Schwab, C.: Quadrature for hp–Galerkin BEM in $\mathbb{R}^3$. Numer. Math. **78**, 211-258 (1997)

[SS04] Sauter, S., Schwab, C.: Randelementmethoden: Analyse, Numerik und Implementierung schneller Algorithmen. B.G. Teubner, Stuttgart, Leipzig, Wiesbaden (2004)

[SZ92] Sokolowski, J., Zolesio, J.-P.: Introduction to Shape Optimization. Springer (1992)